

University of Plymouth

PEARL

<https://pearl.plymouth.ac.uk>








Faculty of Science and Engineering

School of Geography, Earth and Environmental Sciences

2022-09-12



Sequential Lonsdaleite to Diamond Formation in Ureilite Meteorites via *In Situ* Chemical Fluid/Vapor Deposition

Andrew G. Tomkins^{a,1} , Nicholas C. Wilson^b , Colin MacRae^b , Alan Salek^c , Matthew R. Field^d, Helen E. A. Brand^e, Andrew D. Langendam^{a,e}, Natasha R. Stephen^f , Aaron Torpy^b, Zsanett Pintér^a , Lauren A. Jennings^a, and Dougal G. McCulloch^{c,d} 

Edited by Timothy Grove, Massachusetts Institute of Technology, Cambridge, MA; received May 22, 2022; accepted August 5, 2022

Ureilite meteorites are arguably our only large suite of samples from the mantle of a dwarf planet and typically contain greater abundances of diamond than any known rock. Some also contain lonsdaleite, which may be harder than diamond. Here, we use electron microscopy to map the relative distribution of coexisting lonsdaleite, diamond, and graphite in ureilites. These maps show that lonsdaleite tends to occur as polycrystalline grains, sometimes with distinctive fold morphologies, partially replaced by diamond + graphite in rims and cross-cutting veins. These observations provide strong evidence for how the carbon phases formed in ureilites, which, despite much conjecture and seemingly conflicting observations, has not been resolved. We suggest that lonsdaleite formed by pseudomorphic replacement of primary graphite shapes, facilitated by a supercritical C-H-O-S fluid during rapid decompression and cooling. Diamond + graphite formed after lonsdaleite via ongoing reaction with C-H-O-S gas. This graphite > lonsdaleite > diamond + graphite formation process is akin to industrial chemical vapor deposition but operates at higher pressure (~1–100 bar) and provides a pathway toward manufacture of shaped lonsdaleite for industrial application. It also provides a unique model for ureilites that can reconcile all conflicting observations relating to diamond formation.

diamond | lonsdaleite | ureilite | meteorite | chemical vapor deposition

Ureilites are primitive achondrite meteorites that are residues of fractional melt extraction from deep within the ureilite parent body (UPB) (1). Because the UPB underwent extensive melting and had a diameter that may have been >530 km (2), it was likely a dwarf planet (massive enough to form a spheroid under hydrostatic equilibrium; for comparison, the diameter of the impact-modified spheroid Vesta is 525 km), and these meteorites are therefore our only large suite of samples from the mantle of such a body.

Up to 7% graphite occurs in all ureilites, abundant diamond occurs among graphite in most, and evidence for the presence of lonsdaleite has also been reported (3–5). Lonsdaleite is a hexagonal form of diamond that was first reported in 1967 in the Canyon Diablo and Goalpara meteorites (6), has been found in the Popigai impact structure (7, 8), and evidence for this phase has also been found in the diffraction signatures in the products of experiments that subjected graphite to static (9, 10) or shock (11) compression. Although it has recently been suggested that lonsdaleite does not exist as a discrete material in nature (but is instead defective cubic diamond dominated by twinning and stacking faults, given that these defects would produce the diffraction signatures of lonsdaleite) (12, 13), more recent studies have confirmed its rapid production in experiments at 50 GPa (14). The main challenge in confirming that lonsdaleite exists in nature has been a lack of samples that contain large enough crystallites that can be unambiguously identified (note, however, that coarse 0.5–5 μm natural lonsdaleite has been reported from the Kumdykol diamond deposit, North Kazakhstan, although no geological context was provided (15)).

It is also unclear how the various phases of carbon formed in ureilites. Some diamond/lonsdaleite features are said to be consistent with having formed by shock (3, 16–19), based on TEM observations that carbon phases are crystallographically related. The observation that diamonds are found in weakly and moderately shocked ureilites, whereas high degrees of shock are thought to be required, is a conundrum (17). This has been explained by a combination of longer shock durations and catalysis of diamond growth by Fe-Ni and Fe-Si alloys or liquids (17–19); specifically, it has been noted that the diamonds observed in low shock ureilites cannot form without catalysis by metal (17). This is problematic because ureilites are strongly metal depleted, and although some primary metal does occur along grain boundaries and with graphite, it rarely surrounds graphite-diamond grains (20) (see more below). The metal-catalysis pathway also requires temperatures exceeding ~1,350°C (see figure 12

Significance

We report on lonsdaleite and diamond formation in ureilite meteorites, which likely come from the mantle of a destroyed inner solar system dwarf planet. In these meteorites, folded graphite crystals have been pseudomorphed by lonsdaleite. This occurred at mildly elevated pressures through reaction between graphite and supercritical C-H-O-S fluids. Ongoing reaction during cooling then promoted partial replacement of lonsdaleite by diamond + graphite. This process is akin to industrial chemical vapor deposition but operates at higher pressure (~1–100 bar) and provides a pathway toward manufacture of shaped lonsdaleite for industrial application.

Author affiliations: ^aSchool of Earth, Atmosphere and Environment, Monash University, Melbourne, VIC 3800, Australia; ^bCSIRO Mineral Resources, Microbeam Laboratory, VIC 3169, Australia; ^cPhysics, School of Science, RMIT University, Melbourne, VIC 3001, Australia; ^dRMIT Microscopy and Microanalysis Facility, RMIT University, Melbourne, VIC 3001, Australia; ^eAustralian Synchrotron, Clayton, VIC 3168, Australia; and ^fPlymouth Electron Microscopy Centre, University of Plymouth, Drake Circus, Plymouth, PL4 8AA, United Kingdom

Author contributions: A.G.T., D.G.M., N.C.W., C.M. designed research; A.G.T., N.C.W., C.M., A.S., M.R.F., H.E.A.B., A.D.L., N.R.S., A.T., L.A.J., and D.G.M. performed research; A.G.T., N.C.W., C.M., A.S., M.R.F., H.E.A.B., A.T., Z.P., L.A.J., and D.G.M. analyzed data; and A.G.T., D.G.M. wrote the paper.

The authors declare no competing interest.

This article is a PNAS Direct Submission.

Copyright © 2022 the Author(s). Published by PNAS. This article is distributed under [Creative Commons Attribution-NonCommercial-NoDerivatives License 4.0 \(CC BY-NC-ND\)](https://creativecommons.org/licenses/by-nc-nd/4.0/).

¹To whom correspondence may be addressed. Email: andy.tomkins@monash.edu.

This article contains supporting information online at [http://www.pnas.org/lookup/suppl/doi:10.1073/pnas.2208814119/-DCSupplemental](https://www.pnas.org/lookup/suppl/doi:10.1073/pnas.2208814119/-DCSupplemental).

Published September 12, 2022.

in Nakamuta et al. (17)), whereas there is no evidence that such temperatures were ever reached (equilibration temperatures were 70–200°C cooler (1)). The observed strong enrichment of noble gases in ureilite diamonds and lack in coexisting graphite has also been difficult to reconcile with a shock origin (21, 22). The high noble gas content led to suggestions that the diamonds formed through chemical vapor deposition (CVD) in the solar nebula prior to incorporation into the UPB (23–26). However, exposure of nebular diamond to the high temperature of the mantle (1,050–1,280°C (1)) under equilibrium conditions in an asteroid- or dwarf planet-sized UPB would transform it into graphite (27), ruling this possibility out. Furthermore, experiments have shown that diamond formed under shock in closed systems (but not open systems) retains more noble gas than coexisting graphite (26). It has also been found that noble gas isotopes vary as a function of olivine Mg#, and thus oxidation state, which implies that diamonds formed locally and not prior to formation of the UPB (28). The large sizes of some ureilite diamonds (exceeding 100 μm), and the composition of mineral inclusions therein, have been used to argue against the shock and CVD hypotheses, and instead that they formed at >20 GPa in the mantle of a

planetary body considerably larger than Mercury (25, 29). Are the ureilites really from such a large body? If not, and many assume the UPB was closer to 500 km diameter (2, 28, 30), there is currently no satisfactory explanation for diamond and lonsdaleite formation in ureilites.

In this paper, we show that lonsdaleite does exist in some ureilites, and map the relative distribution of graphite, diamond, and lonsdaleite. To do this, we examined carbon-associated textures in 18 ureilites (*SI Appendix, Table S1*), using electron probe microanalysis (EPMA) coupled with transmission electron microscopy (TEM), optical petrography, and synchrotron X-ray diffraction (SXRD) (*Materials and Methods*). We build upon our recent work showing that a C-H-O-S fluid/gas phase pervaded most ureilites during impact disruption (2) to investigate lonsdaleite and diamond formation mechanisms.

Graphite, Diamonds, and the Largest Lonsdaleite Crystals Yet Found in Meteorites. Of the 18 ureilites examined, all contain graphite, most contain diamond, and a small number contain lonsdaleite. Three ureilites contain coarsely crystalline graphite with internal cleavage foliation defining distinctive fold shapes,

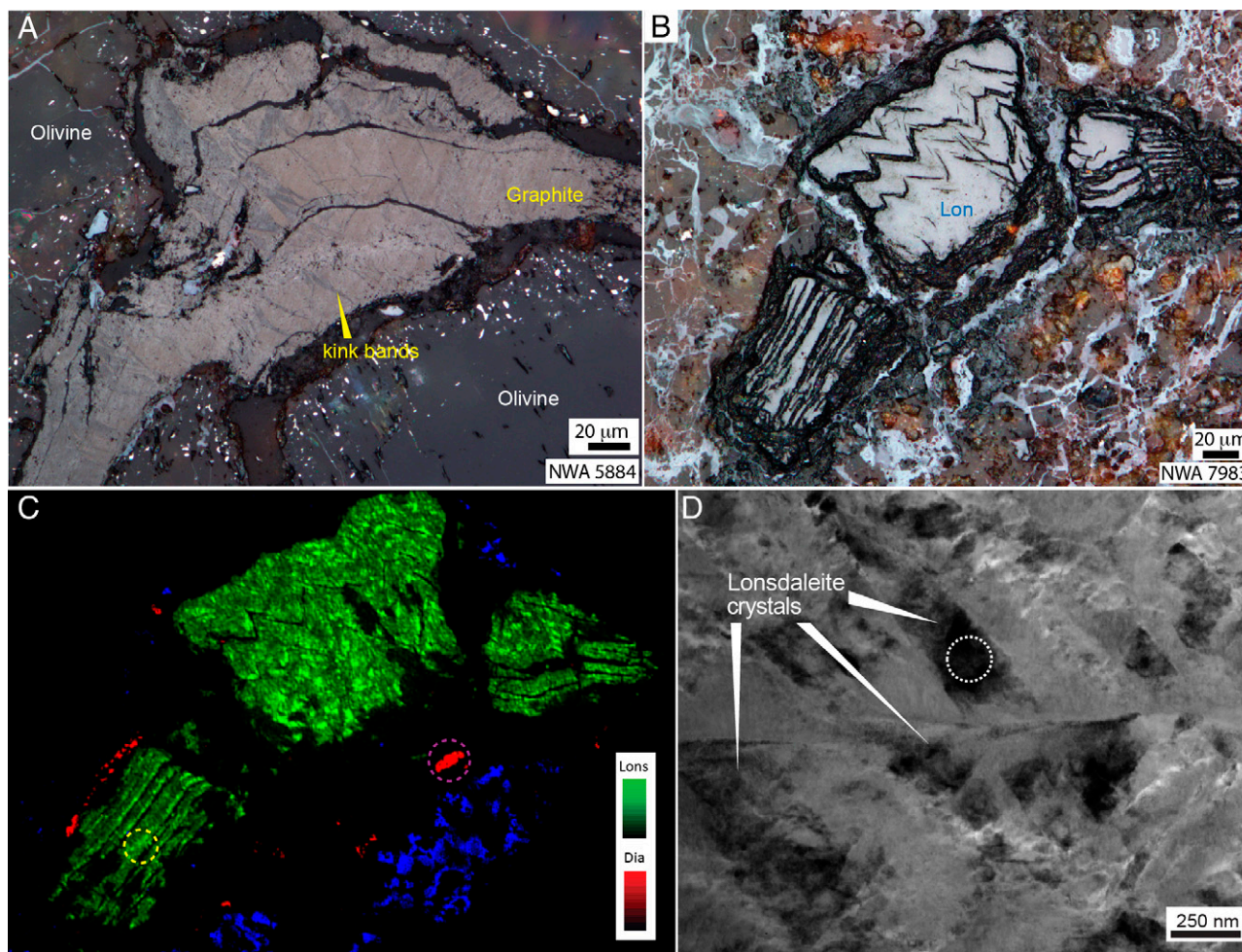


Fig. 1. Images of graphite, lonsdaleite, and diamond in ureilites. (A) Reflected light image showing folded crystalline graphite, with fold morphology defined by graphite cleavage (*SI Appendix, Fig. S1*). Different shading in the graphite is produced by axial planar kink bands. (B) Reflected light image (stacked foci) showing an example of the inherited fold morphology preserved in lonsdaleite (*SI Appendix, Fig. S4*). (C) CL map of the same area as (B) indicating different phases of carbon, where the green regions (from a fit of the 2.317 eV peak; *SI Appendix, Fig. S3*) are lonsdaleite and the red areas (from a fit of the 2.157 eV peak) on the periphery (including the purple dashed circle) are cubic diamond (blue is the CL response from olivine). (D) Scanning TEM Image of a region cut out of the area indicated by yellow circle in (C), highlighting dark lonsdaleite crystals. The diffraction pattern for white area circled is further examined in *SI Appendix, Fig. S5 B–F*. An example of a TEM image of lonsdaleite from NWA 2705 is shown in *SI Appendix, Fig. S5A*.

and no diamonds or lonsdaleite, sitting at well-equilibrated olivine and pyroxene grain boundaries (Fig. 1A and *SI Appendix, Fig. S1 and Table S1*). In these meteorites, there is a small proportion of primary FeNi metal and troilite (FeS) sitting as narrow veins along some grain boundaries, and this is in contact with only a small proportion of the primary graphite (*SI Appendix, Fig. S1A*). The coarse crystalline graphite has been reported previously in several other ureilites and is generally considered to represent the peak metamorphic state of carbon prior to impact modification (31, 32). We agree: the coarsely crystalline, mildly folded, diamond-free graphite flakes sitting around well-equilibrated silicate grain boundaries is what would be expected of the primary metamorphic texture that existed at the termination of the peak metamorphic melt extraction process.

Most of the ureilites that we studied (15) contain clusters of small diamonds embedded in graphite (e.g., Fig. 2 A–C), as is widely reported for ureilites in general (see Meteoritical Bulletin Database). Diamond grain size varies between meteorites, and in the samples examined here, range up to ~20 μm. Individual clusters can be over 600 μm across containing tens to hundreds of diamond grains, constrained by the dimensions of the enclosing graphite. In these meteorites, graphite grains can contain variable abundances of diamonds, with diamond-free and diamond-rich

patches adjacent in some meteorites. In most samples, the majority of diamond clusters are situated in elongate grain boundary graphite domains, with a proportion hosted in distinctly transgressive vein/fracture systems (e.g., Fig. 2 B and C). In the dominant majority of diamond + graphite clusters in most ureilites, there is no primary FeNi metal or troilite in contact with the cluster, or minimal contact at one end of the cluster, in no spatial relationship with the distribution of diamond (e.g., Fig. 2 A and B), and importantly, this is well exemplified by the lowest shock ureilite that we examined, NWA 4225 (*SI Appendix, Fig. S2*).

The well-defined folding of graphite grains shown in Fig. 1A is comparable in texture to equivalently sized polycrystalline lonsdaleite grains in NWA 5996 and NWA 7983 (lonsdaleite was found in 4 ureilites; *SI Appendix, Table S1*). In these meteorites, the foliation-and-fold texture is defined by polycrystalline lonsdaleite (Fig. 1 B and C and *SI Appendix, Figs. S3 and S4*) with the largest individual crystallites yet found in meteorites (some exceeding 500 nm), as determined by TEM (Fig. 1D and *SI Appendix, Figs. S5–S8*). Similar features in NWA 7983 were recently described by Nestola et al. (18), although they referred to the material we have identified as lonsdaleite as nanodiamond (they noted that it has the characteristics of lonsdaleite in micro X-ray powder diffraction spectra, but did not

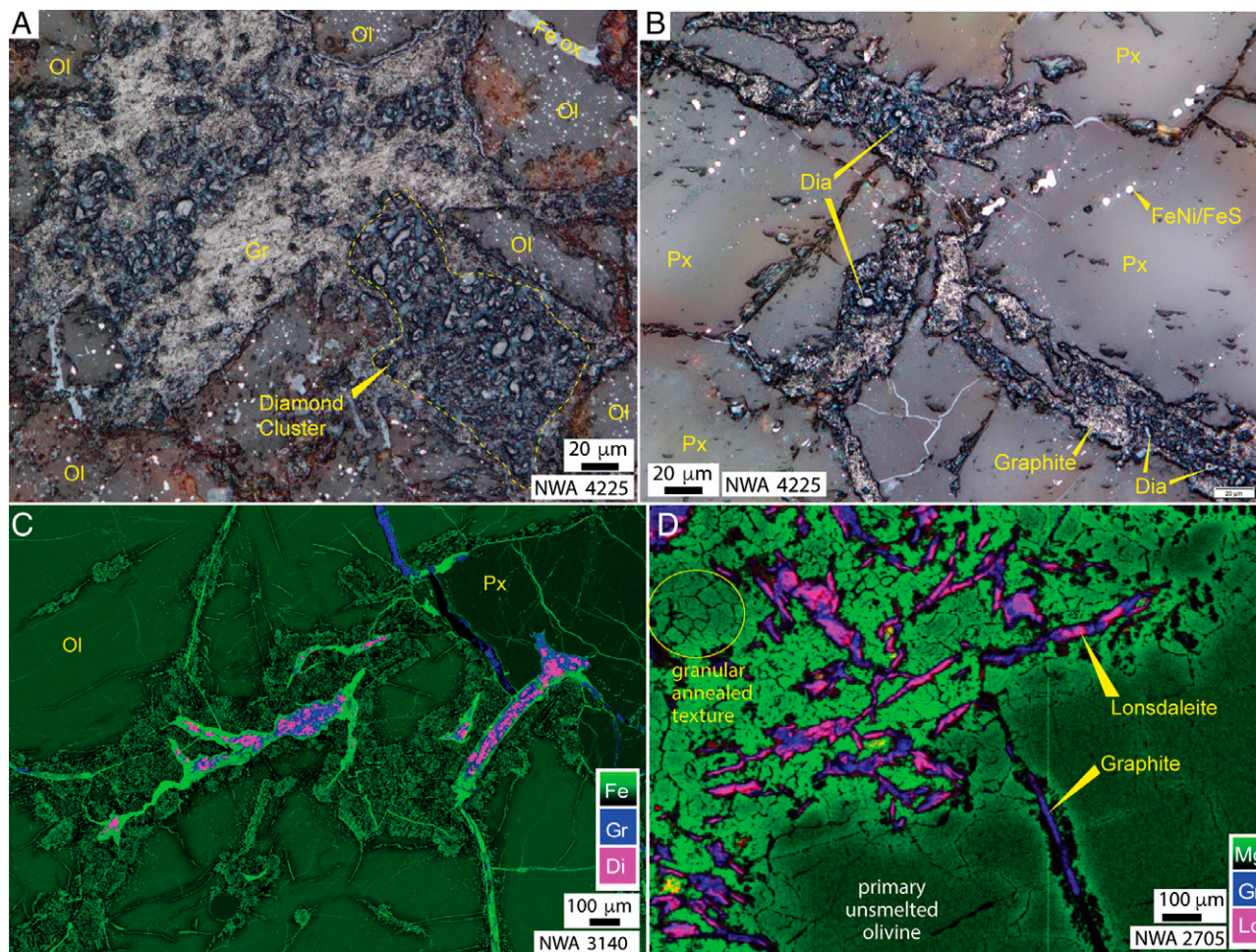


Fig. 2. Textural settings of transgressive lonsdaleite- and diamond-bearing veins in ureilite meteorites. The diamond and lonsdaleite in the element-CL maps are distinguished by thresholding of the CL signal (*Materials and Methods* and *SI Appendix, Fig. S3*). (A) Reflected light image (stacked foci) showing the typical character of cluster diamond in graphite, with varying abundance. (B) Graphite + diamond veins cutting across a single pyroxene crystal. (C) An RGB element-CL map (red = CL 2.157 eV peak; green = Fe; blue = carbon) showing diamond (purple) clusters in graphite (blue) in transgressive veinlets that cut across primary olivine in the zone of stippled smelting. Fe depletion around fracture-associated smelting can also be seen. (D) An RGB element-CL map (red = CL 2.317 eV peak; green = Mg; blue = carbon) showing vein-like arrays of lonsdaleite (purple) and graphite (blue) in annealed and smelted olivine (light green), with primary unsmelted olivine in dark green.

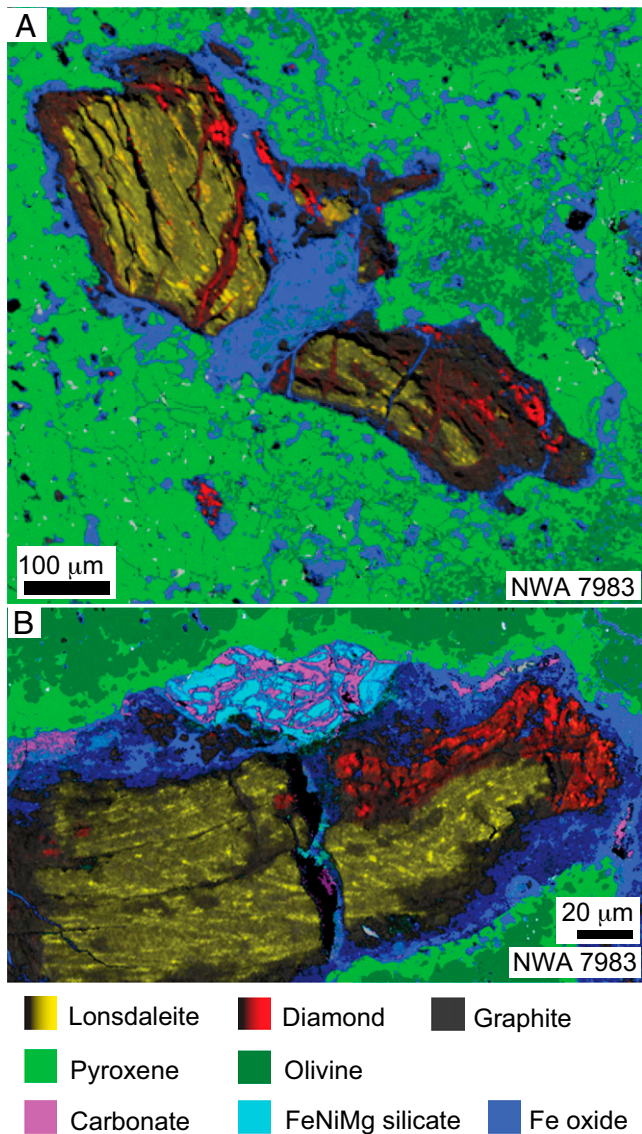


Fig. 3. Mineral maps highlighting the partial replacement of lonsdaleite by diamond (lonsdaleite and diamond distinguished by CL peak fitting, *Materials and Methods*). (A) A large domain of polycrystalline lonsdaleite is cut by a veinlet of diamond, and there are localized clusters of diamond around the margin of the lonsdaleite. (B) Here, a large, foliated, polycrystalline lonsdaleite grain is partially rimmed by numerous diamond grains embedded in graphite.

perform TEM to confirm). Our SXRD analysis of NWA 7983 also confirmed the presence of lonsdaleite (*Materials and Methods* and *SI Appendix*, Fig. S9). These polycrystalline lonsdaleite grains have the same size, shape, and distribution as the graphite in the diamond/lonsdaleite-free ureilites. In both NWA 5996 and NWA 7983, there are clusters of small equant diamonds in graphite partially surrounding most lonsdaleite occurrences, and in places, diamond sits in well-defined microveins cross-cutting the lonsdaleite texture (Fig. 3 and *SI Appendix*, Fig. S4 E and F). One other ureilite, NWA 2705, contains large, distinctly elongate lonsdaleite grains that have vein-like shapes (Fig. 2D and *SI Appendix*, Fig. S5A).

A small number of ureilites provide crucial insights into the formation of lonsdaleite. The intense polysynthetic shock twinning of olivine and pyroxene seen in some ureilites postdates peak metamorphism (otherwise it would have recrystallized), as does the unannealed mosaicism and undulose extinction in olivine in more weakly shocked samples. Lonsdaleite is found in samples with well-developed annealing—either the entire meteorite is

annealed or annealing is focused around the carbon phases (see also (33))—and all samples we examined with strong annealing contain lonsdaleite. Annealed domains are mildly to strongly reduced relative to the primary grains. Importantly, annealing has recrystallized part of the polysynthetic shock twinning in NWA 2705 and NWA 11755, and lonsdaleite is only found in the annealed domains (Fig. 2D). This association therefore implies that lonsdaleite formed after the primary shock event in these meteorites, in association with the reduction and annealing process. In theory, annealing could occur when shock creates numerous subgrains that are then annealed, or shock could create highly strained crystal lattices that are subsequently annealed into subgrains. The textures in NWA 2705 and NWA 11755 indicate that the latter applies.

Olivine and pyroxene are fully annealed into subgrains (*cf.* (33, 34)) in the other two lonsdaleite-bearing ureilites, NWA 5996 and NWA 7983. Pervasive, intense reduction of the olivine, known as smelting (35–39) (see more below), also occurred during this annealing (34), as indicated by intergrown FeNi metal, troilite, and FeO-depleted olivine and pyroxene. These two fully annealed meteorites have a texture akin to that described for the fine-grained porous ureilites of Almahatta Sitta, which have been pervasively reduced (40, 41). We support the previous interpretations (33, 34) that this whole-sample, fine-grained texture was caused by annealing, because the outlines of large preexisting silicate grains are clearly visible. It must have occurred at high temperature because pigeonite and evidence of silicate melting are found in the fine-grained assemblage (41). Because the entire fine-grained assemblage is comprehensively reduced, it is not the product of shock, it is the product of pervasive geochemical reduction.

Effects of Impact Disruption of the Ureilite Parent Body.

At peak metamorphism in the UPB, with different samples recording temperatures between 1,050 and 1,280°C (1) at pressures >150 bar (2), melt extraction and grain boundary equilibration would have left numerous coarse graphite flakes at silicate grain boundaries (time step 1 in Fig. 4), many of which would have had folded shapes clearly delineated by the strong graphite cleavage. This is well exemplified by the textures in NWA 5884 and NWA 5391 (Fig. 1A and *SI Appendix*, Fig. S1). However, uniquely, ureilites contain overprinting “smelting textures,” which reflect reduction of olivine, triggered by a dramatic drop in pressure caused by catastrophic impact disruption of the UPB while the mantle was at, or very near, peak temperature (1, 35–38) (time step 2 in Fig. 4). They consist of localized domains of Fe-depleted olivine containing numerous μm -scale Fe metal and FeS particles. These textures developed around graphite (39) and along fractures and grain boundaries. The predominant development of these textures along fracture arrays and grain boundaries (2, 33, 40), and the extensive addition of sulfur, are clear indications that gas/fluid addition drove much of the reduction (2). We recently showed that the gas/fluid responsible contained H_2 , CH_4 , S_2 , and H_2S , with O derived from oxidation of silicates during smelting, creating a locally varying mix of gas/fluid molecules in the system C-H-O-S (2).

Transgressive veins and vein-networks of graphite are seen in most ureilites and also require a secondary mobilization process that drove textural disequilibrium. The same interpretation was made by Day et al. (42). We suggested that the pressure decrease associated with impact disruption drove exsolution of the C-H-O-S fluid from residual melt, and this fluid then produced the vein and vein-network textures during the smelting process (2). The key point is that these textures formed at low pressures in the

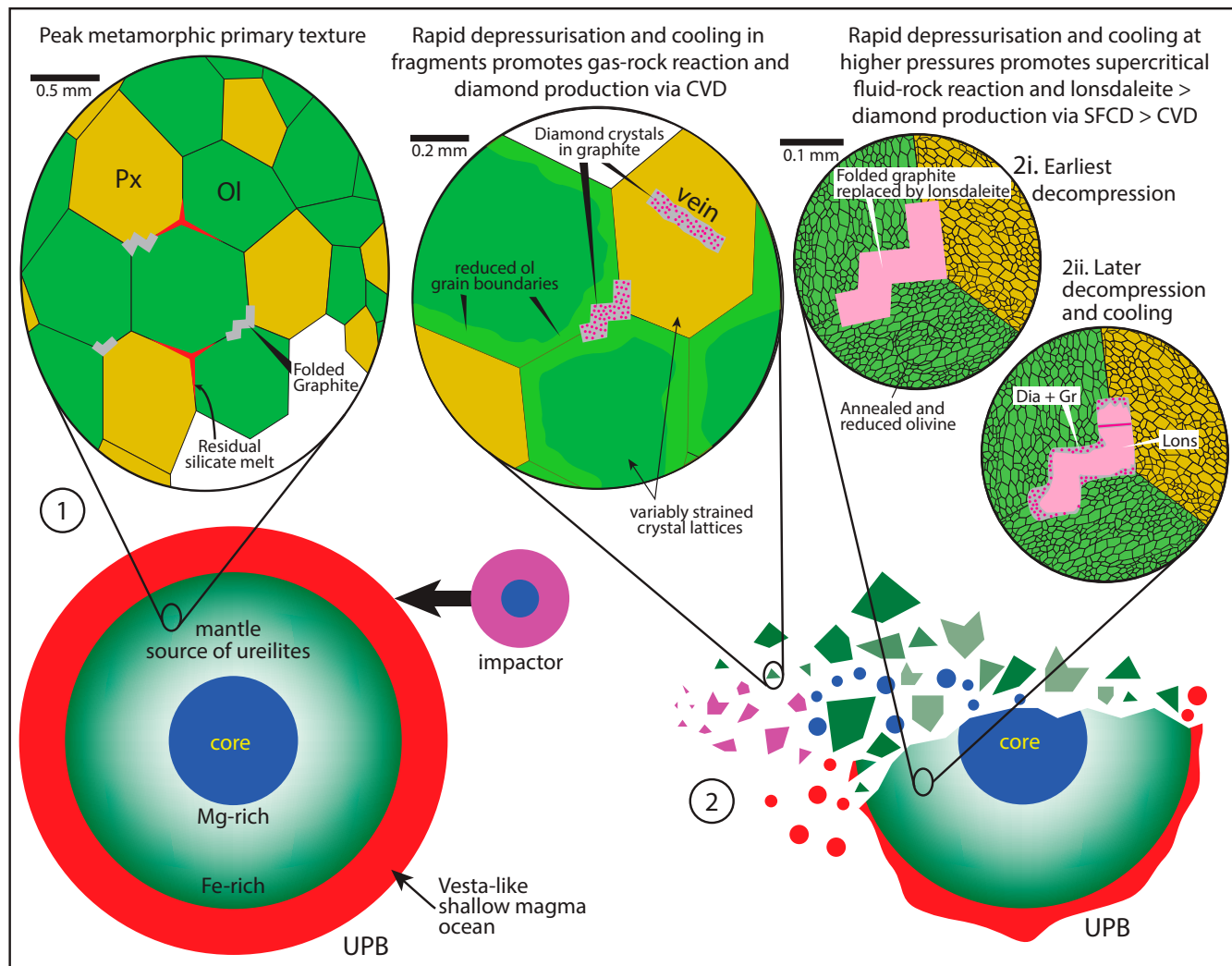


Fig. 4. Schematic diagram illustrating the evolution of the UPB and meteorites derived from it, and the postshock timing of diamond and lonsdaleite formation. Time step 1 (Left) represents the situation prior to impact disruption. At this point, the ureilite core and shallow magma ocean had segregated, leaving the mantle from which ureilites are predominantly derived. This primary mantle consisted of mainly olivine (Ol) and pyroxene (Px), up to 7% graphite, and a small amount of residual silicate, FeNi metal, and sulfide melt (each melt was immiscible). Time step 2 (Right) is when all of the post-impact processes discussed in the paper occurred. These were all driven by the decompression caused by impact disruption; i.e., after the shock event. Pressure decrease caused volatile exsolution from residual melts during adiabatic cooling, and these volatiles then drove smelting (reduction of olivine) and, we argue, diamond and lonsdaleite formation by CVD and possibly SFCD—see text. In larger fragments and the remaining UPB, pressure may have been high enough to allow supercritical fluids to initially be stable, facilitating pseudomorphic replacement of folded graphite by lonsdaleite (SFCD; 2i), and then with cooling, this fluid evolved to gas promoting partial replacement of lonsdaleite by diamond + graphite at rims and in cross cutting veinlets (CVD; 2ii).

immediate aftermath of the catastrophic shock event, and there are many examples where intense shock features are overprinted by secondary annealing associated with smelting (2). Diamond clusters in graphite are interpreted here to have formed during smelting, because they occur in transgressive, smelting-associated veins in multiple samples (Fig. 2 B and C). Since smelting and vein formation occurred at low pressure after the shock event, the diamonds must also have formed postshock.

The interpretation that ureilite diamonds formed under hydrostatic equilibrium at high pressure in a large planetary embryo (sic. >20 GPa (29)) was ruled out on the basis that the textural associations between diamonds, graphite, and surrounding silicates are entirely inconsistent with diamond formation by equilibration at high pressure in the mantle of a planet (18). We agree: static equilibration of carbon at high P-T conditions would tend to form large (mm sized) single diamond crystals (e.g., as seen on Earth), rather than clusters of numerous small diamonds (mostly <20 μm) partially and irregularly replacing graphite.

Here, we suggest that an alternative diamond and lonsdaleite formation mechanism operated via a process akin to industrial CVD at moderate to low pressures immediately after the catastrophic impact disruption event. Below, we argue that this mechanism is more likely than the currently popular model that they were produced at high shock pressure. This idea of diamond CVD during cooling of the UPB has not previously been suggested, and so was not considered in recent models (18, 29); nebular CVD has been ruled out on reasonable grounds (29).

Post-impact Diamond and Lonsdaleite Growth by CVD. To form diamond via CVD, graphite sp^2 bonds must be suppressed in favor of, or converted to, diamond sp^3 bonds. In industrial CVD, this is achieved using a gas mix that includes hydrogen, which destabilizes graphite sp^2 bonds in favor of diamond sp^3 bonds at high temperature (43). Synthetic diamonds are manufactured at conditions of 700–1,100°C and 0.5–101.3 kPa (0.005–1 bar), imposed on mixtures of CH_4 in hydrogen and other gases, which causes deposition onto a substrate (a variety

can be used, including diamond and graphite). Below 700°C, diamond deposition rates are lower, so less useful to industrial manufacture, whereas above 1,100°C, graphite growth starts to dominate (43) (both graphite and diamond are deposited under hotter conditions, up to at least 2,700°C). In some industrial CVD processes, graphite, diamond, and lonsdaleite form together (44).

Diamond formation by CVD occurs in a narrow region of the C-H-O phase diagram (*SI Appendix, Fig. S10*) that straddles the H-CO mixing line (45), so mixtures of H₂-CH₄-CO are ideal. This process is similar to a series of reactions we suggested for gas/fluid-driven smelting in ureilites, where infiltrating H₂, CH₄, S₂, and H₂S drove reduction of olivine and pyroxene to Fe metal and FeS (2). Smelting thus created a spatially variable mixture of CH₄, H₂, H₂S, CO, and H₂O, produced by redox reactions either side of the *f*O₂ required for carbon deposition. Maintenance of low XH₂O conditions during cooling in the UPB is implied by the lack of hydrous silicates in ureilites and the presence of aromatic hydrocarbons among graphite and diamond (16, 46, 47), which likely evolved via reaction between the C-H-O-S fluid/gas and graphite (2). Within that spatially varying mix, there would be domains that fall within the diamond stability window of *SI Appendix, Fig. S10*.

Given the widespread addition of sulfur seen in ureilite smelted domains (2), sulfur was likely an active participant in attaining the conditions needed for diamond stability (*SI Appendix, Fig. S10 B and C*), and experiments exploring the effects of H₂S in industrial CVD show that diamond growth is enhanced at lower temperatures when sulfur is present; referred to as sulfur-assisted CVD (48, 49). Indeed, some sulfur-assisted CVD experiments are conducted in CH₄-H₂S-H₂ gas mixtures (50), and others with CS₂ (51), akin to those envisaged here for ureilites.

Nestola et al. (18) suggested that coarse diamond in NWA 7983, and “nanodiamond” with textures akin to the polycrystalline lonsdaleite pseudomorphs of graphite that we describe, formed during a prolonged shock-induced high-pressure pulse (4–5 s at 150 kbar, 1,250–1,350°C) catalyzed by liquid Fe-Ni-C. However, we note that this mechanism only proceeds at the limits of plausible impact conditions within thin films of Fe-Ni-C melt, whereas our observations have found that there are numerous examples in low shock ureilites where widespread development of microdiamonds occurs in the absence of, or unrelated to, FeNi metal (e.g., Fig. 2 *A and B* and *SI Appendix, Fig. S2*). Because C-H-O-S gas/fluid would be dispersed along all fractures and grain boundaries, post-shock diamond and lonsdaleite formation provides a better explanation of why these have partially replaced *all* graphite grains throughout most ureilites (*SI Appendix*). Pseudomorphism is also a common feature of fluid-mediated dissolution-precipitation reactions in many geological systems (52). The unavoidable change in gas/fluid P-T-X conditions during decompression also provides an explanation for the progressive evolution from lonsdaleite to diamond seen in NWA 7983 and NWA 5996 (i.e., the diamond rims around lonsdaleite and cross-cutting diamond microveins in Fig. 3).

As expressed conceptually in Fig. 4, the low pressures used in industrial CVD would certainly be reached in small fragments of the UPB generated during impact disruption (<12 km diameter for <1 bar), but large fragments, and the likely surviving residual UPB (53), would unavoidably have had higher internal pressures (*SI Appendix, Fig. S11*). As yet, there has been no experimental study of diamond or lonsdaleite formation from a volatile phase at these higher P-T conditions.

Lonsdaleite Formation by Supercritical Fluid Chemical Deposition (SFCVD)? The C-H-O-S fluid/gas in ureilites appears to have progressively evolved during decompression as it exsolved from residual silicate melt (2). At the P-T conditions relevant to deeper parts of the UPB at the onset of impact disruption (1,050–1,280°C, 150 – >1,000 bar (1, 2, 30)), a CH₄-H₂S-H₂-CO mix with minor H₂O would be supercritical (relevant critical points are: H₂, 13 bar, –240°C; CH₄, 46 bar, –83°C; CO₂, 74 bar, 31°C; CS₂, 79 bar, 279°C; H₂S, 90 bar, 100°C; H₂O, 218 bar, 374°C). As disruption, depressurization and cooling progressed in different-sized fragments and the remaining parent body (we showed that rapid cooling would occur in all UPB fragments by adiabatic compensation (2)), local systems would have equilibrated toward a variety of final internal pressures, resulting in an evolution from supercritical fluid to gas at a variety of rates (i.e., during time step 2 in Fig. 4). The critical point of mixtures can be estimated from the mean of the critical temperatures and pressures of the components, but here we have no constraints on the proportions of components. It is, however, clear that sulfur and hydrogen were present, and methane is strongly implied, so the critical point may have been between 46 and 90 bar, which, at the density of ureilites, equates to the center of an 80–112 km diameter UPB fragment (*SI Appendix, Fig. S11*). Although these are plausible fragment sizes for catastrophic disruption of a >500 km UPB, most fragments would be smaller than 80 km, so the final mix was likely gaseous in most cases.

We suggest that lonsdaleite may have formed by reaction between supercritical fluid and preexisting graphite in some larger UPB fragments and the remaining UPB (time step 2i in Fig. 4), accounting for its relative scarcity. Evidence is provided by the textures in NWA 5996 and NWA 7983. Most of the crystalline graphite grains in these two samples have been partially replaced in such a way that lonsdaleite has pseudomorphed the graphite microstructure, even preserving the intricate details of the preexisting foliation, folds, and kinked fabric (Fig. 1 *A–C* and *SI Appendix, Fig. S4*). This lonsdaleite pseudomorphism has in places resulted in small but recognizable localized volume increases (*SI Appendix, Fig. S4C*). Shock-induced conversion of graphite to lonsdaleite or diamond produces a large volume decrease reflecting their respective densities (graphite = 2.26 g/cm³, lonsdaleite and diamond = 3.52 g/cm³), so the observed volume increase requires addition of carbon, such as by fluid-mediated pseudomorphism.

In the meteorites examined here, polycrystalline lonsdaleite tends to occur in fully annealed ureilites (NWA 5996, NWA 7983), or in domains of annealing associated with smelting (NWA 2705, NWA 11755), which formed after the primary shock event. Annealing would normally be taken to imply that these meteorites remained hotter for longer than ureilites lacking annealing (33), and thus that they came from larger fragments of the UPB (under the principle of radiative cooling). But this is not possible because annealed ureilites contain uninverted pigeonite and have measured extremely rapid cooling rates (40, 41, 54). Instead, as we suggested recently (2), a supercritical fluid would tend to drive annealing despite rapid cooling because fluids are highly effective at promoting recrystallization through enhancing diffusion (55–57). In addition, the observation that reduction is relatively mild in annealed domains (lesser FeO depletion of olivine) (34, 58) implies higher pressures because progression of olivine reduction to lower FeO requires lower pressures (2). In sufficiently large UPB fragments, the system would evolve from supercritical fluid to gas with cooling and decompression (time step 2ii in Fig. 4), and this may explain why diamond-graphite clusters and diamond-bearing veins

overprint lonsdaleite. Whether or not a supercritical fluid was involved, this lonsdaleite > diamond transition must be associated with cooling.

Support for our suggestion that the lonsdaleite and diamonds formed by a CVD-like process is provided by previously published Raman spectroscopy data, which show that ureilite diamonds have spectra that are consistent with low pressure CVD and inconsistent with formation by shock (24). Furthermore, experimental work (59) has shown that during growth by CVD in a H₂-CH₄-Ar gas mix, diamond traps at least 20 times more Ar than graphite, matching the observed relative noble gas distribution between these phases in ureilites. Our interpretation is also consistent with the work showing that noble gas isotopes in diamond vary as a function of olivine Mg#, and thus oxidation state and position in the UPB mantle (28). This observation indicates that diamond formed in the presence of a noble gas-bearing fluid/gas phase that had not migrated large distances. Our model thus provides the only known solution to the problem of needing to form lonsdaleite and diamond in situ throughout the UPB mantle fragments during rapid cooling, without the need for catalyzing metal enveloping diamond + graphite.

Although SFC D is known to be more effective than CVD for some industrial processes (57), it has not demonstrated experimentally for lonsdaleite/diamond. We suggest that given the large sizes of the lonsdaleite crystallites we have found, the possibly superior hardness relative to diamond, and the shape-preserving tendency of the process, SFC D may be a pathway to industrial manufacture of shaped lonsdaleite and diamond.

Materials and Methods

Eighteen ureilite samples (*SI Appendix, Table S1*) were examined via optical microscopy, and this was used as a basis for selecting specific samples for detailed analysis by EPMA and TEM. After combined EPMA and TEM work had highlighted the textural differences between diamond and lonsdaleite, we found that optical microscopy could be used to broadly distinguish between lonsdaleite, diamond, and graphite at a larger scale, allowing numerous grains to be examined. Graphite is easily distinguished from diamond and lonsdaleite in reflected light imaging because the latter are hard and sit proud on the surface, whereas graphite is soft and therefore recessive. The reflected light images of these minerals shown in Figs. 1 and 2 and *SI Appendix, Figs. S1, S2, and S4* were obtained by automated stacking of digital images taken at successive optical foci; this allows diamond, lonsdaleite, and graphite to be imaged in focus in the same photomicrograph. Diamond tends to sit in granular clusters among graphite, whereas lonsdaleite tends to somewhat partially pseudomorph pre-existing graphite shapes.

Selected graphite-diamond and graphite-lonsdaleite-diamond-bearing domains were examined using a JEOL 8530F-CL HyperProbe at the CSIRO Microprobe Laboratory in Melbourne. The EPMA was equipped with an optical grating spectrometer, xCLentV (xCLent (60)), for cathodoluminescence (CL) collection and analysis, and a JEOL SXES (SS-9400SXES) extensively modified by CSIRO (61). CL and SXES (soft X-ray emission spectrometry) were used to characterize the textural associations between diamond and lonsdaleite as identified by TEM and to construct a series of element, CL, and SXES maps characterizing the key textures. The optical spectrometer collected from 199 to 972 nm and had a 200 nm entrance slit. Operating conditions were 7 kV, 80 nA, and a dwell per pixel of 400 ms, and maps were collected by scanning the stage with a step size and spot size of 500 nm. We found that, although both proved to be suitable, CL provided the greater contrast than SXES in distinguishing between lonsdaleite and diamond (*SI Appendix, Fig. S12*). Thresholding of the CL spectra (*SI Appendix, Fig. S3*) allowed integration with element maps to highlight the relative distribution of graphite, diamond, and lonsdaleite among silicates. Diamond is distinguished from lonsdaleite by their respective features in the CL spectral response, which makes imaging their relative distribution straightforward. The CL peak at 2.157 eV was selected as being characteristic of diamond, whereas the peak at 2.317 eV was selected to highlight lonsdaleite in the maps of the ureilites examined (*SI Appendix, Fig. S3*). We compared spectra

collected at room temperature with those collected with the stage cooled by liquid nitrogen. The nitrogen-cooled stage collects CL spectra with enhanced and narrower peaks in the case studied here. However, we found that the data collected at ambient temperature were adequate to distinguish diamond from lonsdaleite. Graphite does not have a CL response but appears in maps of carbon distribution. We do not distinguish between crystalline graphite and amorphous carbon. These multi-spectral maps were used to produce element-CL maps (in Fig. 2 C and D and *SI Appendix, Fig. S4*) and phase distribution maps (in Fig. 3 and *SI Appendix, Figs. S3 and S4*), where each mineral is assigned a unique color based on its unique spectral signature, highlighting the relative distribution of coexisting minerals.

Point analyses of olivine and pyroxene were collected from seven ureilite samples to conduct Cr thermometry and estimate the peak metamorphic conditions for inclusion, along with existing thermometry data, in *SI Appendix, Table S1*. Minerals were analyzed on the JEOL 8530F-CL HyperProbe under a focused beam with a voltage of 15 kV and an average probe current of 15 nA. All elements were measured for 20 s (10 s on the background), except Na which was measured for 10 s (5 s on the background). Oxide abundances were collected simultaneously from four spectrometers. Thermometry was conducted following the method of Collinet and Grove (1), which is based on the exchange of Cr between coexisting olivine and orthopyroxene or pigeonite.

For the TEM work, site-specific lamellae were cut from areas of different CL brightness within the hard diamond/lonsdaleite grains using a FEI Scios dual beam focused ion beam (FIB) instrument. The lamellae were lifted out of the sample using a tungsten needle attached to the micromanipulator system, while remaining in the focused ion beam chamber (so-called “in situ plucking”). After attaching to Cu grids, the lamellae were thinned with progressively lower Ga beam energies down to 2 kV to minimize specimen damage. The lamellae were analyzed on either a JEOL 2100F or JEOL F200 transmission electron microscopes operating at both 80 and 200 kV. No evidence of significant electron beam damage was observed at either accelerating voltage. The camera length of all diffraction patterns was calibrated using polycrystalline Pt, available on each lamella from the protective surface layer deposited during FIB processing. Electron energy loss spectroscopy (EELS) was undertaken on a JEOL F200 transmission electron microscope fitted with a Gatan Enfinitum spectrometer. The energy resolution obtained from the full width at half maximum of the zero loss peak was 0.5 eV. EELS spectrum images (maps) were taken in scanning TEM mode with a probe size of ~1 nm. Spectrum images in the low loss regime and in the vicinity of the carbon k edge of up to 500 × 500 pixels were collected. Each low loss spectrum was deconvoluted to remove plural scattering using the Fourier ratio method (62). A density map was then created by determining the maximum energy of the bulk plasmon peak for each spectrum and then converting this to density (63).

To further confirm that lonsdaleite is present in NWA 7986—the primary focus of our TEM work—we conducted SXRD analysis at the powder diffraction beamline of the Australian Synchrotron. The beamline was set up in reflection geometry with a 5° incident angle and a beam size of 1 mm horizontally and 0.75 mm vertically (footprint of ~1 × 3 mm on the sample), using a nominal energy of 21 keV, with the wavelength refined using NIST SRM LaB₆ 660b to be 0.589376(2). Datasets were collected using the Mythen II microstrip detector (64). Paired patterns, with the detector set 0.5° apart, each of 60 s, were collected to cover gaps between detector modules. We took 83 datasets in steps across the sample, covering an area of 20 × 9 mm in the center of the sample block with a small amount of overlap in neighboring datasets (~0.5 mm). Datasets were merged using PDVPeR, in-house software available at the beamline. These patterns (e.g., *SI Appendix, Fig. S9*) were then analyzed using the search-match capabilities of Malvern Highscore Pro with the ICDD PDF4+ database.

Data, Materials, and Software Availability. All study data are included in the article and/or supporting information.

ACKNOWLEDGMENTS. EPMA was conducted at the CSIRO Microbeam Laboratory. TEM, SEM, and FIB milling were conducted at the RMIT Microscopy and Microanalysis Facility (RMMF). SXRD was conducted at the Powder Diffraction beamline of the Australian Synchrotron. The authors gratefully acknowledge funding from ARC FT180100533 and ARC LE130100087. We thank Junnel Alejandro and Cameron Davidson for making high-quality polished thin sections and mounts of our diamond-bearing samples. The editors and reviewers are thanked for their efforts in handling and reviewing the manuscript.

1. M. Collinet, T. L. Grove, Incremental melting in the ureilite parent body: Initial composition, melting temperatures, and melt compositions. *Meteorit. Planet. Sci.* **55**, 832–856 (2020).
2. A. L. Langendam *et al.*, CHOS gas/fluid-induced reduction in ureilites. *Meteorit. Planet. Sci.* **56**, 2062–2082 (2021).
3. N. Nakamura, S. Toh, Transformation of graphite to lonsdaleite and diamond in the Goalpara ureilite directly observed by TEM. *Am. Mineral.* **98**, 574–581 (2013).
4. D. W. Mittlefehldt, T. J. McCoy, C. A. Goodrich, A. Kracher, in (*Planetary Materials Reviews in Mineralogy*, 1998), ed. by J. J. Papike, vol. 36, (Mineralogical Society of America), p. 4.14.195.
5. C. A. Goodrich *et al.*, Origin and history of ureilitic material in the solar system: The view from asteroid 2008 TC3 and the Almahata Sitta meteorite. *Meteorit. Planet. Sci.* **50**, 782–809 (2015).
6. R. E. Hanneman, H. M. Strong, F. P. Bundy, Hexagonal diamonds in meteorites: Implications. *Science* **155**, 995–997 (1967).
7. A. Yeliseyev, S. Gromilov, V. Afanasiev, I. Sildos, V. Kiisk, Effect of lonsdaleite on the optical properties of impact diamonds. *Diam. Relat. Mater.* **101**, 107640 (2020).
8. W. Baek *et al.*, Unique nanomechanical properties of diamond–lonsdaleite biphasic: Combined experimental and theoretical consideration of Popigai impact diamonds. *Nano Lett.* **19**, 1570–1576 (2019).
9. F. P. Bundy, J. S. Kasper, Hexagonal diamond—A new form of carbon. *J. Chem. Phys.* **46**, 3437–3446 (1967).
10. F. P. Bundy *et al.*, The pressure-temperature phase and transformation diagram for carbon; updated through 1994. *Carbon* **34**, 141–153 (1996).
11. D. Kraus *et al.*, Nanosecond formation of diamond and lonsdaleite by shock compression of graphite. *Nat. Commun.* **7**, 10970 (2016).
12. P. Németh *et al.*, Lonsdaleite is faulted and twinned cubic diamond and does not exist as a discrete material. *Nat. Commun.* **5**, 5447 (2014).
13. V. A. Greshnyakov, E. A. Belenkov, Investigation on the formation of lonsdaleite from graphite. *J. Exp. Theor. Phys.* **124**, 265–274 (2017).
14. S. J. Turneaure, S. M. Sharma, T. J. Volz, J. M. Winey, Y. M. Gupta, Transformation of shock-compressed graphite to hexagonal diamond in nanoseconds. *Sci. Adv.* **3**, eaao3561 (2017).
15. T. G. Shumilova, E. Mayer, S. I. Isaenko, Natural monocrystalline lonsdaleite. *Dokl. Earth Sci.* **441**, 1552–1554 (2011).
16. C. Le Guillou, J. N. Rouzaud, L. Remusat, A. Jambon, M. Bourrot-Denise, Structures, origin and evolution of various carbon phases in the ureilite Northwest Africa 4742 compared with laboratory-shocked graphite. *Geochim. Cosmochim. Acta* **74**, 4167–4185 (2010).
17. N. Nakamura, F. Kitajima, K. Shimada, In situ observation, X-ray diffraction and Raman analyses of carbon in ureilites: Origin and formation mechanisms of diamond in ureilites. *J. Mineral. Petrol. Sci.* **111**, 252–269 (2016).
18. F. Nestola *et al.*, Impact shock origin of diamonds in ureilite meteorites. *Proc. Natl. Acad. Sci. U.S.A.* **117**, 25310–25318 (2020).
19. A. Barbaro *et al.*, Origin of micrometer-sized impact diamonds in ureilites by catalytic growth involving Fe-Ni-silicide: The example of Kenna meteorite. *Geochim. Cosmochim. Acta* **309**, 286–298 (2021).
20. C. A. Goodrich, R. B. Ash, J. A. Van Orman, K. Domanik, W. F. McDonough, Metallic phases and siderophile elements in main group ureilites: Implications for ureilite petrogenesis. *Geochim. Cosmochim. Acta* **112**, 340–373 (2013).
21. I. Gyollai *et al.*, A combined petrographic and micro-Raman study of meteoritic microdiamond in ALH-77257 ureilite and ALH-78113 aubrite. *Spectrosc. Lett.* **45**, 151–155 (2012).
22. V. K. Rai, S. V. S. Murty, U. Ott, Nitrogen in diamond-free ureilite Allan Hills 78019: Clues to the origin of diamond in ureilites. *Meteorit. Planet. Sci.* **37**, 1045–1055 (2010).
23. K. Fukunaga, J. Matsuda, K. Nagao, M. Miyamoto, K. Ito, Noble-gas enrichment in vapour-growth diamonds and the origin of diamonds in ureilites. *Nature* **328**, 141–143 (1987).
24. M. Miyamoto, J.-i. Masamichi, K. Ito, Raman spectroscopy of diamond in ureilite and implication for the origin of diamond. *Geophys. Res. Lett.* **15**, 1445–1448 (1988).
25. M. Miyahara *et al.*, Unique large diamonds in a ureilite from Almahata Sitta 2008 TC 3 asteroid. *Geochim. Cosmochim. Acta* **163**, 14–26 (2015).
26. J.-i. Matsuda, A. Kusumi, H. Yajima, Y. Syono, Noble gas studies in diamonds synthesized by shock loading in the laboratory and their implications on the origin of diamonds in ureilites. *Geochim. Cosmochim. Acta* **59**, 4939–4949 (1995).
27. C. S. Kennedy, G. C. Kennedy, The equilibrium boundary between graphite and diamond. *J. Geophys. Res.* **81**, 2467–2470 (1974).
28. M. W. Broadley, D. V. Bekaert, B. Marty, A. Yamaguchi, J.-A. Barrat, Noble gas variations in ureilites and their implications for ureilite parent body formation. *Geochim. Cosmochim. Acta* **270**, 325–337 (2020).
29. F. Nabeie *et al.*, A large planetary body inferred from diamond inclusions in a ureilite meteorite. *Nat. Commun.* **9**, 1327 (2018).
30. P. H. Warren, Parent body depth–pressure–temperature relationships and the style of the ureilite anatexis. *Meteorit. Planet. Sci.* **47**, 209–227 (2012).
31. C. A. Goodrich, Ureilites: A critical review. *Meteoritics* **27**, 327–352 (1992).
32. J. L. Berkley, J. H. Jones, Primary igneous carbon in ureilites: Petrological implications. *J. Geophys. Res. Solid Earth* **87**, A353–A364 (1982).
33. A. E. Rubin, Shock, post-shock annealing, and post-annealing shock in ureilites. *Meteorit. Planet. Sci.* **41**, 125–133 (2006).
34. P. H. Warren, A. E. Rubin, Pyroxene-selective impact smelting in ureilites. *Geochim. Cosmochim. Acta* **74**, 5109–5133 (2010).
35. J. L. Berkley, The nature and origin of ureilites. *Geochim. Cosmochim. Acta* **44**, 1579–1597 (1980).
36. S. K. Sinha, R. O. Sack, M. E. Lipschutz, Ureilite meteorites: Equilibration temperatures and smelting reactions. *Geochim. Cosmochim. Acta* **61**, 4235–4242 (1997).
37. D. Walker, T. Grove, Ureilite smelting. *Meteoritics* **28**, 629–636 (1993).
38. H. Downes, D. W. Mittlefehldt, N. T. Kita, J. W. Valley, Evidence from polymict ureilite meteorites for a disrupted and re-accreted single ureilite parent asteroid gardened by several distinct impactors. *Geochim. Cosmochim. Acta* **72**, 4825–4844 (2008).
39. P. H. Warren, H. Huber, Ureilite petrogenesis: A limited role for smelting during anatexis and catastrophic disruption. *Meteorit. Planet. Sci.* **41**, 835–849 (2006).
40. J. S. Herrin *et al.*, Thermal and fragmentation history of ureilitic asteroids: Insights from the Almahata Sitta fall. *Meteorit. Planet. Sci.* **45**, 1789–1803 (2010).
41. M. Horstmann, A. Bischoff, The Almahata Sitta polymict breccia and the late accretion of asteroid 2008TC3. *Chem. Erde* **74**, 149–183 (2014).
42. J. M. D. Day *et al.*, A carbon-rich region in Miller Range 091004 and implications for ureilite petrogenesis. *Geochim. Cosmochim. Acta* **198**, 379–395 (2017).
43. M. Schwander, K. Partes, A review of diamond synthesis by CVD processes. *Diam. Relat. Mater.* **20**, 1287–1301 (2011).
44. B. K. Roul, B. B. Nayak, P. K. Mishra, B. C. Mohanty, Diamond and diamond-like-carbon growth on Si (100) by hot filament-assisted RF plasma CVD. *J. Mater. Synth. Process.* **7**, 281–288 (1999).
45. P. K. Bachmann, D. Leers, H. Lydtin, Towards a general concept of diamond chemical vapour deposition. *Diam. Relat. Mater.* **1**, 1–12 (1991).
46. D. P. Glavin *et al.*, Extraterrestrial amino acids in the Almahata Sitta meteorite. *Meteorit. Planet. Sci.* **45**, 1695–1709 (2010).
47. H. Sabbah, A. L. Morrow, P. Jenniskens, M. H. Shaddad, R. N. Zare, Polycyclic aromatic hydrocarbons in asteroid 2008 TC3: Dispersion of organic compounds inside asteroid. *Meteorit. Planet. Sci.* **45**, 1710–1717 (2010).
48. H. Sternschulte, M. Schreck, B. Stritzker, A. Bergmaier, G. Dollinger, Growth and properties of CVD diamond films grown under H₂S addition. *Diam. Relat. Mater.* **12**, 318–323 (2003).
49. F. Piazza *et al.*, Diamond film synthesis at low temperature. *Diam. Relat. Mater.* **15**, 109–116 (2006).
50. S. Gupta, B. R. Weiner, G. Morell, Influence of sulfur incorporation on field-emission properties of microcrystalline diamond thin films. *J. Mater. Res.* **18**, 2708–2716 (2003).
51. M. A. Sampaio *et al.*, Electrical properties of diamond films prepared from carbon disulfide and ethanol in hydrogen. *Vacuum* **85**, 180–183 (2010).
52. A. Putnis, Mineral replacement reactions. *Rev. Mineral. Geochem.* **70**, 87–124 (2009).
53. N. Rai, H. Downes, C. Smith, Ureilite meteorites provide a new model of early planetesimal formation and destruction. *Geochim. Perspect. Lett.* **14**, 20–25 (2020).
54. T. Mikouchi *et al.*, Electron microscopy of pyroxene in the Almahata Sitta ureilite. *Meteorit. Planet. Sci.* **45**, 1812–1820 (2010).
55. L. E. Aradi *et al.*, Fluid-enhanced annealing in the subcontinental lithospheric mantle beneath the westernmost margin of the Carpathian-Pannonian extensional basin system. *Tectonics* **36**, 2987–3011 (2017).
56. J. Zhao, J. Brugger, B. A. Grguric, Y. Ngathai, A. Pring, Fluid-enhanced coarsening of mineral microstructures in hydrothermally synthesized bornite-digenite solid solution. *ACS Earth Space Chem.* **1**, 465–474 (2017).
57. M. Majjmel, S. Marre, E. Garrido, C. Aymonier, Supercritical fluid chemical deposition as an alternative process to CVD for the surface modification of materials. *Chem. Vap. Depos.* **17**, 342–352 (2011).
58. M. Zolensky *et al.*, Mineralogy and petrography of the Almahata Sitta ureilite. *Meteorit. Planet. Sci.* **45**, 1618–1637 (2010).
59. K. Fukunaga, J.-i. Matsuda, K. Nagao, M. Miyamoto, K. Ito, Noble-gas enrichment in vapour-growth diamonds and the origin of diamonds in ureilites. *Nature* **328**, 141–143 (1987).
60. C. M. Macrae, N. C. Wilson, S. A. Johnson, P. L. Phillips, M. Otsuki, Hyperspectral mapping-combining cathodoluminescence and X-ray collection in an electron microprobe. *Microw. Res. Tech.* **67**, 271–277 (2005).
61. C. M. Macrae, N. C. Wilson, A. Torpy, Hyperspectral cathodoluminescence. *Mineral. Petrol.* **107**, 429–440 (2013).
62. R. F. Egerton, *Electron Energy-Loss Spectroscopy in the Electron Microscope* (Springer, 2011), pp. 491.
63. A. C. Ferrari *et al.*, Density, sp³ fraction, and cross-sectional structure of amorphous carbon films determined by x-ray reflectivity and electron energy-loss spectroscopy. *Phys. Rev. B* **62**, 11089 (2000).
64. B. Schmitt *et al.*, Mythen detector system. *Nucl. Instrum. Methods Phys. Res. A* **501**, 267–272 (2003).